Science
AAAS

Molecular Architecture and Assembly Principles of *Vibrio cholerae* Biofilms

Veysel Berk *et al.*

Science **337**, 236 (2012);
DOI: 10.1126/science.1222981

Science (print ISSN 0036-8075; online ISSN 1095-9203) is published weekly, except the last week in December, by the American Association for the Advancement of Science, 1200 New York Avenue NW, Washington, DC 20005.

30. Z. G. Gao *et al.*, *Mol. Pharmacol.* **63**, 1021 (2003).
31. B. S. Zhorov, V. S. Ananthanarayanan, *J. Biomol. Struct. Dyn.* **15**, 631 (1998).
32. J. Selent *et al.*, *PLoS Comput. Biol.* **6**, e1000884 (2010).
33. M. J. Howard *et al.*, *Mol. Pharmacol.* **32**, 53 (1987).
34. J. M. Nunnari *et al.*, *J. Biol. Chem.* **262**, 12387 (1987).
35. M. Canals *et al.*, *Trends Biochem. Sci.* **36**, 663 (2011).
36. J. P. Changeux, *Annu. Rev. Biophys.* **41**, 103 (2012).
37. T. P. Kenakin, *Br. J. Pharmacol.* **165**, 1659 (2012).
38. B. K. Ho, F. Gruswitz, *BMC Struct. Biol.* **8**, 49 (2008).

Acknowledgments: This work was supported by NIH Common Fund in Structural Biology grant P50 GM073197 for technology development, NIH/National Institute of General Medical Sciences (NIGMS) PSI:Biology grant U54 GM094618 for biological studies and structure production, NIGMS grant R01 GM089857 to V.C., a Dutch Research Council Nederlandse Organisatie voor Wetenschappelijk Onderzoek (NWO) TOP grant (714.011.001: "The crystal structure of the adenosine A_{2A} receptor: The follow-up") to A.P.I., and an NWO Veni grant (11188) to L.H.H. We thank J. Velasquez for help on molecular biology; T. Trinh, K. Allin, and M. Chu for help on baculovirus expression; T. Mulder-Krieger and H. de Vries for their technical expertise in the biochemical characterization, G. van Westen for his educated comments on the crystal structure; M. Mileni for reviewing the final structure; J. P. Changeux for discussions on GPCR allostery and the potential for allosteric stabilizers; K. Kadyshevskaya for assistance with figure preparation; A. Walker for assistance with manuscript preparation; J. Smith, R. Fischetti, and N. Sanishvili for assistance in development and use of the minibeam and beamtime at GM/CA-CAT beamline 23-ID at the Advanced Photon Source, which is supported by National Cancer Institute grant Y1-CO-1020 and NIGMS grant Y1-GM-1104. Coordinates and the structure factors have been deposited in the Protein Data Bank under the accession code (4EIY). R.C.S. is a founder and on the Board of Directors of Receptos, a GPCR structure-based drug discovery company. R.C.S., C.B.R., A.A.T., W.L., F.X., E.C., and V.K. are inventors on a patent applied for jointly by The Scripps Research Institute and Receptos on the use of fusion proteins to crystallize GPCRs.

Supplementary Materials

www.sciencemag.org/cgi/content/full/337/6091/232/DC1
Materials and Methods
Figs. S1 to S10
Tables S1 and S2
References (*39*–*57*)

17 January 2012; accepted 18 May 2012
10.1126/science.1219218

Molecular Architecture and Assembly Principles of *Vibrio cholerae* Biofilms

Veysel Berk,[1,2]* Jiunn C. N. Fong,[3] Graham T. Dempsey,[4] Omer N. Develioglu,[6] Xiaowei Zhuang,[4,5] Jan Liphardt,[1,2,7] Fitnat H. Yildiz,[3]* Steven Chu[8]*†

In their natural environment, microbes organize into communities held together by an extracellular matrix composed of polysaccharides and proteins. We developed an in vivo labeling strategy to allow the extracellular matrix of developing biofilms to be visualized with conventional and superresolution light microscopy. *Vibrio cholerae* biofilms displayed three distinct levels of spatial organization: cells, clusters of cells, and collections of clusters. Multiresolution imaging of living *V. cholerae* biofilms revealed the complementary architectural roles of the four essential matrix constituents: RbmA provided cell-cell adhesion; Bap1 allowed the developing biofilm to adhere to surfaces; and heterogeneous mixtures of *Vibrio* polysaccharide, RbmC, and Bap1 formed dynamic, flexible, and ordered envelopes that encased the cell clusters.

Microbes within biofilms are more resistant to antibiotics; immune clearance; and osmotic, acid, and oxidative stresses as compared with planktonic cells (*1*–*7*). Despite advances in identifying the polysaccharide and proteinaceous constituents of the biofilm extracellular matrix, the mechanisms by which these factors yield a mechanically defined and spatially organized biofilm are largely unknown (*8*–*10*). *Vibrio cholerae* biofilm formation involves the production of *Vibrio* polysaccharide (VPS) and three matrix proteins (RbmA, RbmC, and Bap1) predicted to contain carbohydrate-binding domains (fig. S1A) (*11*–*13*). To investigate the molecular mechanisms of biofilm development, we used a *V. cholerae* rugose variant with increased capacity to form biofilms (*11*). We inserted Myc, FLAG, and human influenza hemagglutinin epitopes into its genome at the 3′ ends of the *rbmA*, *rbmC*, and *bap1* genes, respectively (fig. S1B), allowing us to label these matrix proteins in vivo by supplementing the growth medium with corresponding cyanine dye–labeled primary antibodies (Fig. 1).

We used four-color confocal imaging to validate this labeling strategy and obtain a diffraction-limited overview of biofilm architecture (Fig. 1, A to C, and movie S1). Cells were mainly organized into elongated clusters whose boundaries were defined by three-dimensional (3D) envelopes of the RbmC (red) and Bap1 (green) proteins (Fig. 1C, red arrow). Within the envelope that encases the cell clusters, the relative Bap1 signal was highest in those areas with the least RbmC (Fig. 1A and figs. S5 and S6). Deletion of either RbmC or Bap1 did not impair cluster formation or the resultant architecture of the envelope (Fig. 1D and fig. S7) (*11*, *14*). The cell clusters had a regular width of 2.2 ± 0.3 μm (n = 42 clusters), whereas their length varied from 2 to 8 μm (fig. S8). Each cell within a cluster contacted the cluster boundary and, thus, the interstitial space between clusters, perhaps facilitating nutrient delivery and waste disposal.

However, although Bap1 and RbmC share 47% peptide sequence similarity (*11*), their spatial distributions differed notably at the interface between the coverslip and the cell clusters (fig. S9). Bap1 was concentrated at the biofilm-surface interface (*14*), whereas RbmC was absent from the interface (Fig. 1, B and C, and fig. S9). Moreover, a *bap1* deletion strain had a more severely altered biofilm phenotype than a *rbmC* deletion strain (*11*, *14*), all pointing to Bap1 having two separable functions—namely, encasing cell clusters and attaching cells to the surface.

In contrast to RbmC and Bap1, we detected RbmA throughout the biofilm (Fig. 1, A to C) (*14*). Strains lacking RbmA have reduced colony corrugation and are less resistant to detergent treatment (*12*) but can still adhere to surfaces. Surprisingly, deletion of *rbmA* caused loss of cell ordering into clusters and associated RbmC-Bap1 envelopes, although both of these proteins were clearly present within the biofilm (Fig. 1D and fig. S7). Thus, Bap1 appears to help the biofilm to adhere to surfaces, RbmC and Bap1 appear to encapsulate cell clusters, and RbmA appears to participate in cell-cell adhesion (movies S2 to S6) (*11*, *12*, *14*)

To further test these hypotheses and learn how biofilms assemble, we imaged living biofilms as they developed from a single founder cell into mature biofilms (Fig. 2A and fig. S10). We followed matrix protein secretion and organization with a continuous in situ immunostaining approach (*15*) in which labeled primary antibodies were added to the growth medium (Fig. 2A). At the time of initial attachment, individual founder cells did not have detectable RbmA, RbmC, and Bap1 on their surface. The first matrix protein to appear postattachment was RbmA, which accumulated at discrete sites on the cell surface. After the first cell division, the newly formed daughter cell remained attached to the founder cell, unlike in planktonic cells, where the two cells quickly separate (Fig. 2A).

Bap1 then appeared at the junction between the two cells and also on the substrate near the cells (Fig. 2A). Bap1 gradually accumulated radially over distances of tens of micrometers from its initial location on or near the founder cell (Fig. 2, A and B). The founder cell and its immediate environment had notably more Bap1 than the rest of the biofilm for the entire 6.5-hour

[1]Department of Physics, University of California, Berkeley, CA 94720, USA. [2]Molecular and Cellular Biology, University of California, Berkeley, CA 94720, USA. [3]Department of Microbiology and Environmental Toxicology, University of California, Santa Cruz, CA 95064, USA. [4]Biophysics Program, Harvard University, Cambridge, MA 02138, USA. [5]Department of Chemistry and Chemical Biology, Department of Physics, and Howard Hughes Medical Institute (HHMI), Harvard University, Cambridge, MA 02138, USA. [6]Department of Otorhinolaryngology, Taksim Training and Research Hospital, Istanbul, Turkey. [7]Physical Biosciences Division, Lawrence Berkeley National Laboratory, Berkeley, CA 94720, USA. [8]U.S. Department of Energy, 1000 Independence Avenue, SW, Washington, DC 20585, USA.

*To whom correspondence should be addressed. E-mail: vberk@berkeley.edu (V.B.); fyildiz@ucsc.edu (F.H.Y.); correspondence to S.C. should be addressed to vberk@berkeley.edu
†Formerly of the Departments of Physics and Molecular and Cellular Biology, University of California, Berkeley, CA 94720, USA.

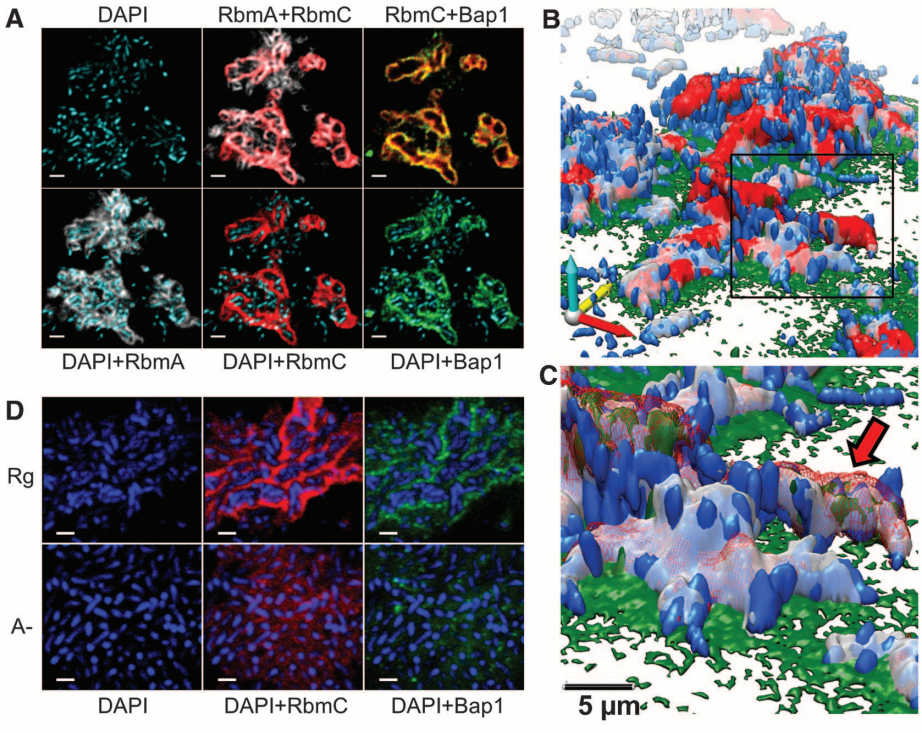

Fig. 1. *V. cholerae* biofilm structure. (**A**) Optical section of biofilm 4 μm above the coverslip. Images are pseudocolored in blue (cells), gray (RbmA), red (RbmC), and green (Bap1). RbmA localizes around and within cell clusters; RbmC and Bap1 encase cell clusters. Cells were counterstained with 4′,6-diamidino-2-phenylindole (DAPI). Scale bars, 3 μm. (**B**) Three-dimensional biofilm architecture. Colors are as in (A). (**C**) Enlargement of the boxed region in (B). The red arrow indicates one cell cluster. The red signal is now rendered partially transparent to allow visualization of cells within an RbmC-containing cluster. (**D**) Comparison of biofilm architecture formed by rugose (Rg) and Δ*rbmA* (A-) strains. RbmA is required for cell cluster formation. Scale bars, 2 μm.

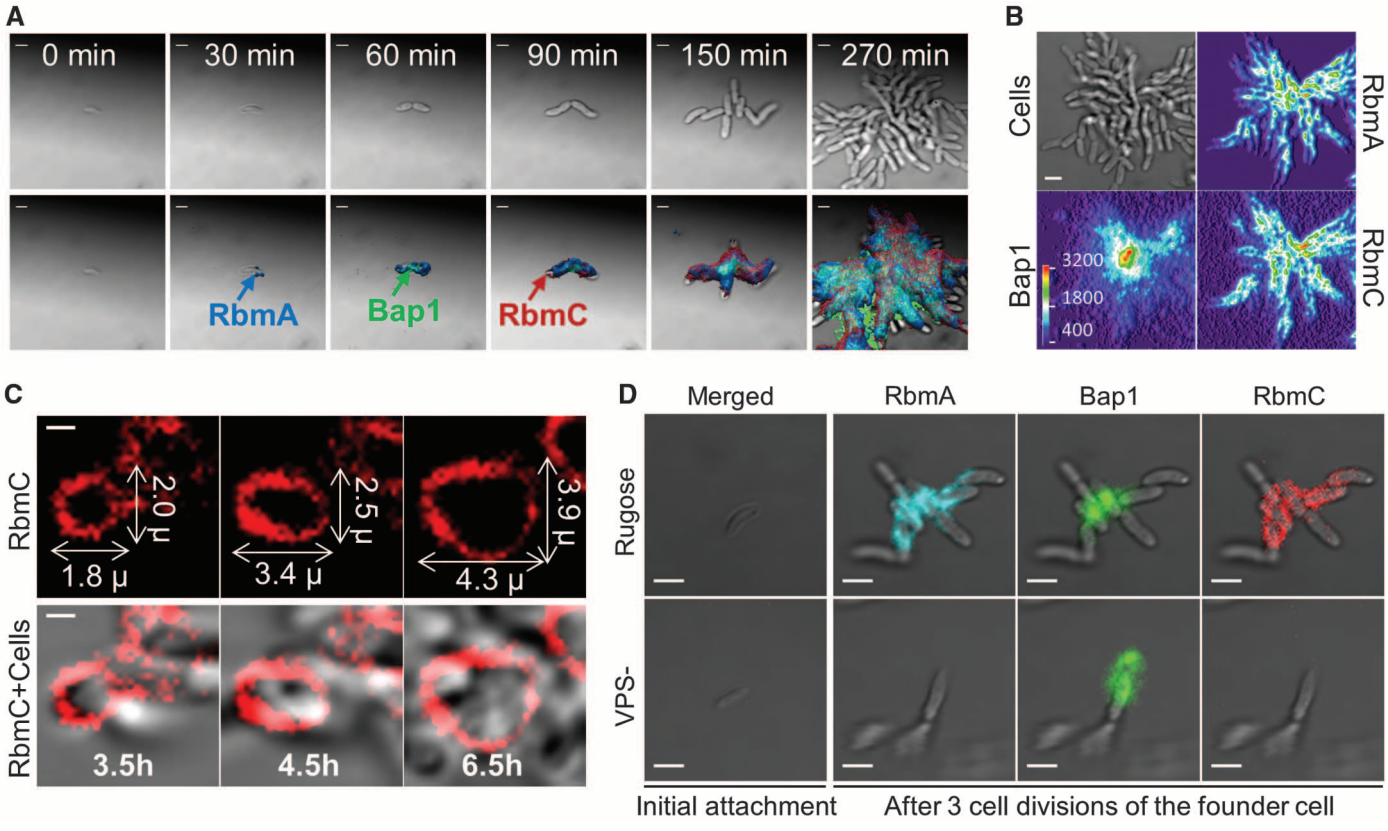

Fig. 2. Time-lapse CLSM imaging of *V. cholerae* biofilm development and cluster formation. (**A**) Expression and subsequent distribution of matrix proteins followed by time-lapse CLSM using continuous direct immunostaining. Cell outlines (bright field) are gray; RbmA, Bap1, and RbmC are shown in blue, green, and red, respectively. Scale bars, 2 μm. (**B**) Bright-field biofilm image and corresponding fluorescent channel surface plots of Bap1, RbmA, and RbmC obtained 4.5 hours postinoculation. Fluorescence intensity is color-coded according to the color scale bar. Bap1 spread from a central point corresponding to the founder cell position, whereas RbmA and RbmC were more homogenously distributed through the biofilm cells. Scale bar, 3 μm. (**C**) Gradual expansion of the RbmC-containing cluster tracked by time-lapse CLSM. Scale bars, 1 μm. (**D**) Inability to produce VPS (VPS-) prevents retention of daughter cells, as well as accumulation of RbmA and RbmC and also blocks biofilm formation. Scale bars, 3 μm.

duration of the experiment. The radially symmetrical distribution of Bap1 relative to the founder cell suggests that Bap1 is continuously secreted into solution by the founder cell and other early members of the young biofilm, after which it accumulates on nearby surfaces (Fig. 2B and fig. S11).

The third matrix protein, RbmC, first appeared after 90 min at discrete sites on the cell surface. Later in biofilm development, the RbmC-Bap1 envelopes formed and then grew by expansion in all directions, with the size of the RbmC-Bap1 envelope doubling within three cell divisions to accommodate the new cell mass (Fig. 2C). Biofilm formation thus involves the temporally sequenced and spatially heterogeneous secretion of matrix proteins, which may have complementary architectural functions—namely, retention of daughter cells after division by RbmA, surface functionalization by Bap1, and encapsulation of the cell clusters by RbmC/Bap1.

Next, we investigated how the RbmC and Bap1 matrix proteins interact with VPS during biofilm formation. VPS is a polysaccharide thought to form a polymeric network that gives mechanical continuity to the biofilm (*8*, *16*–*19*). *V. cholerae* cells lacking either VPS (VPS–) or all three matrix proteins (ABC–) were unable to form 3D biofilms (fig. S12). The parent strain biofilm phenotype could be recovered by coculturing VPS– and ABC– strains, showing that heterologous provision of these four materials is sufficient to restore normal biofilm formation (figs. S1A and S12). VPS– cells could stick to surfaces, but subsequently produced daughter cells did not accumulate and were instead lost in the growth medium (Fig. 2D and movie S5) (*20*). Although RbmA, RbmC, and Bap1 proteins were synthesized (figs. S13 and S14), they did not accumulate on the surface of VPS– cells (Fig. 2D). Bap1 was detected on the substrate near the founder cell (Fig. 2D), as expected if Bap1's main function is to adhere to diverse substrates and tether the biofilm (*14*). Thus, VPS is required for accumulation of the RbmA, RbmC, and Bap1 on the cell surface, which, in turn, is needed for formation of mature biofilms (*13*, *14*).

Because VPS was required for accumulation of matrix proteins on the cell surface, we wondered whether the opposite was also true. We directly stained the VPS with a Cy3-labeled wheat germ agglutinin (WGA), which recognizes *N*-acetylglucosamine sugars in the VPS (*21*). RbmC was essential for sustained incorporation of VPS throughout *V. cholerae* biofilms (fig. S15A). Without RbmC, there were occasional bright dots of VPS within the colony but at a much lower density than in the parent strain biofilm (fig. S15A). Thus, sustained retention of VPS is codependent with retention of RbmC (Fig. 2D and fig. S15). The VPS staining also confirmed that the RbmC/Bap1 envelopes contained VPS, as expected (Fig. 1A and fig. S15B).

Three-dimensional biofilm development requires a specific, mutually interdependent series of protein/VPS synthesis, secretion, capture, and cross-linking steps. However, the ~200-nm spatial resolution of confocal laser scanning microscopy (CLSM) (*22*, *23*) was insufficient to directly visualize these developmental intermediates. We thus constructed a multicolor 3D superresolution imaging apparatus using stochastic optical reconstruction microscopy (*23*–*28*) with a localization precision of 19, 21, and 42 nm in *x*, *y*, and *z* (full width at half maximum) (fig. S16). As before, we added labels to the growth medium and imaged living biofilms. With the use of a Cy3-WGA reagent, VPS was first detected at several discrete sites on the cell surface at time t = 15 min postattachment (Fig. 3A, white arrows). Over the next 2 hours, the number of VPS spots, as well as their intensity, increased slowly. At t = 60 min postattachment, 3D superresolution images of VPS organization showed that the polymer was primarily organized into 50- to 200-nm diameter spheroids protruding away from the cell surface (Fig. 3B, white arrow). It appears that VPS is progressively extruded from the cell as a flexible polymer that, like all relaxed flexible polymers, adopts an isotropic, spherical configuration.

Pseudomonas aeruginosa biofilms have been reported to self-heal within minutes after mechanical disruption beyond their yield point, implying that relatively transient interactions are responsible for maintaining the *P. aeruginosa* matrix (*29*). How could such recovery be possible if the VPS (or Psl in *P. aeruginosa*) were irreversibly cross-linked by matrix proteins such as RbmC? We used two-color 3D superresolution imaging to visualize the organization of VPS and RbmC within a biofilm (*15*). The superresolution microscope has wide dynamic range and can detect single VPS and RbmC molecules. VPS and RbmC were not homogeneously distributed within the mature biofilm, but both matrix components were confined to the envelopes encasing

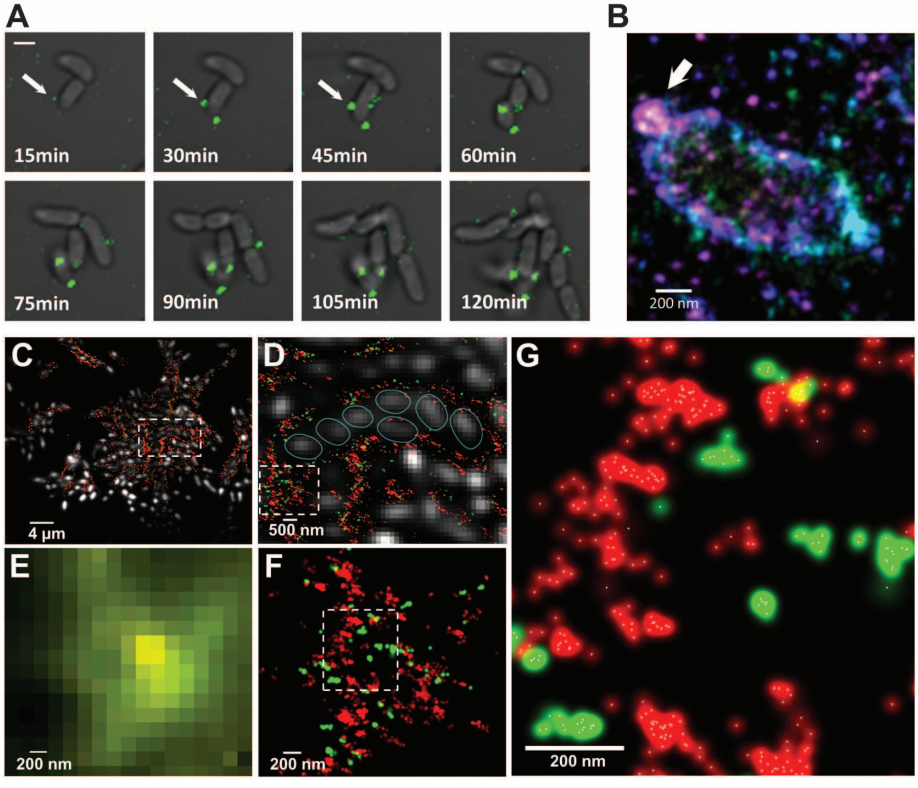

Fig. 3. Exopolysaccharide secretion, initial organization, and molecular architecture of *V. cholerae* biofilms. (**A**) Time-lapse CLSM images of VPS (green) production and secretion in *V. cholerae* cells during biofilm formation. Fluorescent images of VPS are merged with bright-field images of cells. White arrows indicate VPS. Scale bar, 2 μm. (**B**) Three-dimensional superresolution image of a single *V. cholerae* cell. The white arrow indicates a ball-like structure of VPS on the surface of the *V. cholerae* cell early in biofilm formation. Color corresponds to height: −300 nm (violet) to +300 nm (red). (**C**) Three-dimensional two-color superresolution image (200-nm z-section) of a rugose variant biofilm showing molecular organization of VPS (red) and RbmC (green) around cell clusters. Cells were counterstained with DAPI (white). (**D**) Enlarged boxed region in (C) showing organization of cells within the VPS/RbmC-enclosed cluster. Individual cells were outlined (light blue) for clarity. (**E**) Enlarged boxed region in (D) as it appears in conventional, diffraction-limited microcopy, showing unresolved VPS and RbmC signals. (**F**) Superresolution image of the same region in (E), showing distribution of RbmC and the VPS polymers in a biofilm matrix. (**G**) Enlarged boxed region in (F). White symbols indicate the center of a Gaussian fit to each localization events.

the cell clusters and to the interstitial space between clusters (Fig. 3, C and D). The mechanism(s) by which bacteria achieve such spatial segregation of materials within the biofilm and, thus, generate a matrix architecture with submicrometer features are unknown. Moreover, most RbmC signal was not uniformly distributed within the VPS matrix (Fig. 3, E to G). Hence, RbmC and VPS may have homophilic (RbmC-RbmC or VPS-VPS) and heterophilic (RbmC-VPS) interactions, where RbmC may act as a reversible cross-linker of VPS. VPS organization must also be dynamic; otherwise, the cells could not sharply repartition RbmC and VPS into the envelopes and interstitial spaces (Fig. 3D).

We used a matrix-labeling strategy to observe in real time as *V. cholerae* biofilms develop with single-protein and single-polymer precision, revealing assembly principles and intermediates. Cells organize into clusters within the biofilm, and the mature biofilm is a composite of these clusters. An envelope composed of VPS, Bap1, and RbmC encloses these clusters, and RbmA is required for their formation. The VPS/Bap1/RbmC envelope is structured on the molecular level by an unknown mechanism(s) and is capable of reforming, stretching, and expanding to accommodate cell growth.

References and Notes

1. J. W. Costerton, P. S. Stewart, E. P. Greenberg, *Science* **284**, 1318 (1999).
2. L. Hall-Stoodley, P. Stoodley, *Trends Microbiol.* **13**, 7 (2005).
3. M. R. Parsek, P. K. Singh, *Annu. Rev. Microbiol.* **57**, 677 (2003).
4. P. S. Stewart, J. W. Costerton, *Lancet* **358**, 135 (2001).
5. T.-F. Mah *et al.*, *Nature* **426**, 306 (2003).
6. G. G. Anderson, G. A. O'Toole, *Curr. Top. Microbiol. Immunol.* **322**, 85 (2008).
7. A. Reisner, N. Høiby, T. Tolker-Nielsen, S. Molin, *Contrib. Microbiol.* **12**, 114 (2005).
8. H.-C. Flemming, J. Wingender, *Nat. Rev. Microbiol.* **8**, 623 (2010).
9. D. López, H. Vlamakis, R. Kolter, *Cold Spring Harbor Perspect. Biol.* **2**, a000398 (2010).
10. M. Harmsen, L. Yang, S. J. Pamp, T. Tolker-Nielsen, *FEMS Immunol. Med. Microbiol.* **59**, 253 (2010).
11. J. C. N. Fong, F. H. Yildiz, *J. Bacteriol.* **189**, 2319 (2007).
12. J. C. N. Fong, K. Karplus, G. K. Schoolnik, F. H. Yildiz, *J. Bacteriol.* **188**, 1049 (2006).
13. J. C. N. Fong, K. A. Syed, K. E. Klose, F. H. Yildiz, *Microbiology* **156**, 2757 (2010).
14. C. Absalon, K. Van Dellen, P. I. Watnick, *PLoS Pathog.* **7**, e1002210 (2011).
15. Materials and methods are available as supplementary materials on *Science* Online.
16. I. W. Sutherland, *Microbiology* **147**, 3 (2001).
17. E. Karatan, P. Watnick, *Microbiol. Mol. Biol. Rev.* **73**, 310 (2009).
18. F. H. Yildiz, X. S. Liu, A. Heydorn, G. K. Schoolnik, *Mol. Microbiol.* **53**, 497 (2004).
19. S. S. Branda, S. Vik, L. Friedman, R. Kolter, *Trends Microbiol.* **13**, 20 (2005).
20. S. Moorthy, P. I. Watnick, *Mol. Microbiol.* **52**, 573 (2004).
21. I. J. Goldstein, C. E. Hayes, *Adv. Carbohydr. Chem. Biochem.* **35**, 127 (1978).
22. J. B. Pawley, B. R. Masters, *J. Biomed. Opt.* **13**, 029902 (2008).
23. S. W. Hell, *Science* **316**, 1153 (2007).
24. M. J. Rust, M. Bates, X. Zhuang, *Nat. Methods* **3**, 793 (2006).
25. E. Betzig *et al.*, *Science* **313**, 1642 (2006).
26. M. Bates, B. Huang, G. T. Dempsey, X. Zhuang, *Science* **317**, 1749 (2007).
27. B. Huang, W. Wang, M. Bates, X. Zhuang, *Science* **319**, 810 (2008).
28. S. T. Hess, T. P. K. Girirajan, M. D. Mason, *Biophys. J.* **91**, 4258 (2006).
29. O. Lieleg, M. Caldara, R. Baumgärtel, K. Ribbeck, *Soft Matter* **7**, 3307 (2011).

Acknowledgments: We thank B. Huang for providing image processing software and D. J. Wozniak, J. H. D. Cate, X. Nan, A. Arkin, and A. Yildiz for critical evaluation of the manuscript. This work is supported by the NSF [grant PHY-0647161 (J.L.)] and the NIH [grants AI055987 (F.H.Y.) and GM096450 and GM068518 (X.Z.)]. X.Z. is a HHMI Investigator. J.L. acknowledges support from the U.S. Department of Energy Office of Basic Energy Sciences (FWP SISGRKN) and Lawrence Berkeley National Laboratory.

Supplementary Materials

www.sciencemag.org/cgi/content/full/337/6091/236/DC1
Materials and Methods
Figs. S1 to S17
Tables S1 and S2
References (*30*–*40*)
Movies S1 to S6

5 April 2012; accepted 22 May 2012
10.1126/science.1222981

Oscillatory Dynamics of Cdc42 GTPase in the Control of Polarized Growth

Maitreyi Das,[1]* Tyler Drake,[2]* David J. Wiley,[1] Peter Buchwald,[1] Dimitrios Vavylonis,[2] Fulvia Verde[1,3]†

Cells promote polarized growth by activation of Rho-family protein Cdc42 at the cell membrane. We combined experiments and modeling to study bipolar growth initiation in fission yeast. Concentrations of a fluorescent marker for active Cdc42, Cdc42 protein, Cdc42-activator Scd1, and scaffold protein Scd2 exhibited anticorrelated fluctuations and oscillations with a 5-minute average period at polarized cell tips. These dynamics indicate competition for active Cdc42 or its regulators and the presence of positive and delayed negative feedbacks. Cdc42 oscillations and spatial distribution were sensitive to the amounts of Cdc42-activator Gef1 and to the activity of Cdc42-dependent kinase Pak1, a negative regulator. Feedbacks regulating Cdc42 oscillations and spatial self-organization appear to provide a flexible mechanism for fission yeast cells to explore polarization states and to control their morphology.

The conserved guanosine triphosphatase (GTPase) Cdc42 establishes cell polarity by regulating the cytoskeletal asymmetry required for normal cell function, differentiation, and motility (*1*, *2*). In budding yeast, Cdc42 breaks the symmetry of spherical cells by clustering in one area of the membrane, the site of bud growth, through a "winner-take-all" positive-feedback mechanism (*3*–*6*). However, such a mechanism cannot explain how multiple growing zones form simultaneously in other cells. Fission yeast cells initially grow in a monopolar fashion, from the tip that existed before division (the old end), and activate bipolar growth that includes the new end as well, once a minimal cell length has been achieved ["new end take off" (NETO)] (*7*). Fission yeast is thus an ideal system to study how Cdc42 is distributed at multiple sites.

To characterize Cdc42 during the transition to bipolar growth, we used a fluorescent fusion protein [Cdc42/Rac interactive binding peptide–green fluorescent protein (GFP), CRIB-GFP] that binds specifically to activated, guanosine triphosphate (GTP)–bound Cdc42 (*8*). In larger bipolar cells, CRIB-GFP intensities at cell ends showed out-of-phase oscillations with an average period of 5 min (Fig. 1, A and B; movies S1 and S2, and tables S2 and S3). Oscillations were detectable in more than 50% of cells (table S2), when imaging every 15 s instead of 1 min (Fig. 1C), and in three dimensions (Fig. 1D). The rest of the cells displayed anticorrelated fluctuations without obvious periodicity. For shorter cells, nongrowing ends still had detectable CRIB-GFP fluorescence, albeit at lower intensities than the older, growing ends (fig. S1). The tip intensities still underwent anticorrelated oscillations and fluctuations, but around asymmetric averages, unlike longer cells (table S2).

We visualized fluorescently labeled scaffold protein Scd2, which is proposed to mediate Cdc42 activation by binding to the Cdc42 GEF (guanine nucleotide exchange factor) Scd1 and to Cdc42 (*9*, *10*). Scd2-GFP intensity at the cell tips oscillated and fluctuated much like CRIB-GFP intensity (fig. S2 and table S2), as did Scd1-3xGFP and Cdc42-GFP (fig. S3). Thus, CRIB-GFP oscillations and fluctuations appear to reflect the activated Cdc42 protein complex.

To understand how GTP-Cdc42 levels might influence the NETO transition, we measured instantaneous cell growth rates along with CRIB-GFP intensity in cells undergoing NETO, which occurs in cells longer than 9 μm (*7*). Intensities at both new and old ends fluctuated strongly over time (Fig. 1E). The instantaneous growth rate was correlated with abundance of CRIB-GFP at both old and new ends; cell tips with a CRIB-GFP tip fraction below 0.2 grew slower than tips with the fraction above 0.2 (Fig. 1F). Varied degrees of asymmetry were also observed at intermediate lengths in a population of asynchronous

[1]Department of Molecular and Cellular Pharmacology (R-189), University of Miami Miller School of Medicine, Post Office Box 016189, Miami, FL 33101, USA. [2]Department of Physics, Lehigh University, 16 Memorial Drive East, Bethlehem, PA, 18015, USA. [3]Marine Biological Laboratory, 7 MBL Street, Woods Hole, MA 02543, USA.

*These authors contributed equally to this work.
†To whom correspondence should be addressed. E-mail: fverde@med.miami.edu